Analysis of Rotor Dynamic by One-Dimensional Variable Kinematic Theories

E. Carrera[1]
Professor of Aerospace Structures and Aeroelasticity
e-mail: erasmo.carrera@polito.it

E. M. Filippi
e-mail: matteo.filippi@polito.it

E. Zappino
e-mail: enrico.zappino@polito.it

Department of Mechanical and Aerospace Engineering,
Politecnico di Torino,
Corso Duca degli Abruzzi 24,
10129 Torino, Italy

In this paper, Carrera's unified formulation (CUF) is used to perform free-vibrational analyses of rotating structures. The CUF is a hierarchical formulation which offers a procedure to obtain refined structural theories that account for variable kinematic description. These theories are obtained by expanding the unknown displacement variables over the beam section axes by adopting Taylor's polynomials of N-order, in which N is a free parameter. Linear case ($N = 1$) permits us to obtain classical beam theories while higher order expansions could lead to three-dimensional description of dynamic response of rotors. The finite element method is used to derive the governing equations in weak form. These equations are written in terms of few fundamental nuclei, whose forms do not depend on the approximation used (N). In order to assess the new theory, several analyses are carried out and the results are compared with solutions presented in the literature in graphical and numerical form. Among the considered test cases, a rotor with deformable disk is considered and the results show the convenience of using refined models since that are able to include the in plane deformability of disks. [DOI: 10.1115/1.4024381]

1 Introduction

Since rotors are the most important part of many machines, their dynamic behavior is a subject worthy of study. In fact, the growing interest in the investigation of characteristics of spinning structures has given considerable impulse to the development of many theories devoted to the analysis of dynamics of shafts, disks, turbine blades, and propellers. In most cases, the rotor is relatively simple and it can be represented as a single beam or a series of beam elements and rigid disks.

The classical beam theory introduced by Euler and Bernoulli has been adopted by many researchers. For instance, Bauer [1] presented an analytical approach to investigate the vibrational behavior of a beam rotating with constant speed about its longitudinal axis for all boundary conditions. About ten years later, Chen and Liao [2] used the assumed-modes approximate method to evaluate how the dynamic behavior of a rotating slender beam is affected by the ratio of moments of inertia of the cross section and the pretwisted angle. Furthermore, by using the same structural model, Banerjee [3] solved the differential equations of motion by extending the field of application of the dynamic stiffness method (DSM) to rotating structures. Unfortunately, these solutions are inadequate for short and stubby bodies in which rotary inertia and shear deformations are important. In order to take into account these effects, more refined theories have been widely employed. In fact, Zu and Han presented [4] analytical solutions for free flexural vibrations of a spinning, finite Timoshenko beam subjected to a moving load for the six classical boundary conditions. In order to consider also elastic supports, Choi et al. [5] presented an efficient and accurate quadrature method for studying the dynamics of a spinning shearable beam. On the other hand, in the framework of DSM, Curti [6,7] analyzed the vibrational behavior of moderate thick shafts by adding rotatory inertia and shear deformation effects to Euler–Bernoulli's model. In Ref. [8], G. J. Sheu and Yang showed that both whirl and critical speeds can be expressed analytically as a function of a geometric parameter (slenderness ratio) of a Rayleigh beam. A further result demonstrates that the number of the critical speeds is limited by the above parameter. Sheu and Chen [9] presented the study of the instability of a cantilevered shaft-disk system subjected to periodic longitudinal forces by means of a lumped mass model able to detect the shear deformation effects.

The increasing use of composite materials in the design of rotors demands the development of adequate and reliable structural models. To handle this problem, Singh and Gupta [10] proposed a refined beam theory formulation by direct reduction from a layerwise shell theory for analyzing the dynamics of composite shafts. To analyze laminated cylindrical shells, Ramezani and Ahmadian [11] combined the above theory and the Wave Propagation Approach, whereas Banerjee [12] employed the DSM. In addition, we can cite Librescu et al. [13–16], who proposed advanced beam formulations for dealing with thin-walled structures made up of both anisotropic and functionally graded materials.

Previously, it was pointed out that rotors are usually modeled as deformable beams with some rigid bodies at certain positions for describing the effects of disks or concentrated masses. However, the rigid body assumption can be unacceptable when these disks are deformable. The complex shapes and unconventional boundary conditions of real rotors have led the researchers to develop suitable finite elements for overcoming these difficulties. For instance, Genta and Tonoli [17,18] proposed that the displacements of a disk can be written as a superimposition of a rigid motion and a deflection relative to the rigid body configuration. In accordance with this assumption, the last contribution was approximated with a truncated Fourier series in the tangential direction whereas, for the radial direction, polynomial functions were used. Jang and Lee [19] combined the finite element method (FEM) with the substructure synthesis in order to describe the dynamic behavior of a spinning disk-spindle system. The disk was modeled by using the Kirchhoff plate theory and von Karman nonlinear strain, while in contrast, the spindle and stationary shaft were described by the Rayleigh and the Euler finite element beam, respectively. Furthermore, Guo et al. [20] conceived a nine-nodes superparametric finite element so as to take into account the geometric nonlinearity due to the large deformation of spinning cylindrical thin shells. Finally, in Ref. [21], the authors evaluated the capabilities of the 3D and 2D Fourier finite elements models for performing analyses of complex rotating machines. In this research, interesting considerations were provided for a correct interpretation of the natural frequencies computed in the rotating frame.

[1]Corresponding author.

Contributed by the Structures and Dynamics Committee of ASME for publication in the Journal of Engineering for Gas Turbines and Power. Manuscript received December 11, 2012; final manuscript received April 29, 2013; published online July 31, 2013. Assoc. Editor: Jerzy T. Sawicki.

A comprehensive overview of the rotor dynamics phenomena and the classical analysis approaches can be found in the work by Rao [22] and Genta [23]. It is clear that refined modeling leads to more accurate results than classical beam models, but the major drawback is the rapidly increasing of degrees of freedom (DOFs). To cope with this issue, one convenient solution could be the development of refined beam theories. Carrera's unified formulation allows us to reach this goal. The procedure makes it possible to consider the order and the types of theories as free input parameters. CUF was first developed for plate and shell models. For instance, in Refs. [24,25], Carrera provided a comprehensive description of possible approaches to plate and shell laminated structures and introduced the unified formulation to obtain several models based on displacements and transverse stress assumptions. Furthermore, finite element implementations were presented by detailing the matrices of the elements. Carrera et al. [26] investigated the static and dynamic behavior of multilayered plates embedding piezolayers by using CUF. The results show that Unified Formulation is able to lead to a quasi-three-dimensional description of global and local characteristics of the piezoelectric plates. Further assessments are presented in Ref. [27], in which the vibrational free response of homogeneous and multilayered simply supported plates is evaluated. Recently, CUF has been extended to the beam model. Carrera and Giunta tested the performance of higher-order theories, by using N-order Taylor type expansions of the section coordinates in order to define the displacement variables [28]. In that paper, analyses were conducted on isotropic beams with rectangular and I-shaped cross sections and the governing differential equations were solved via the Navier-type closed-form solution. Instead, in Ref. [29], displacement unknowns were expanded by using N-order Lagrange polynomials (LE) which were defined on a set of sampling points belonging to the section. Several analyses were also conducted on a square section beam by adopting finite element procedure. Many studies have been devoted to evaluating the capabilities of the new refined finite elements. In Ref. [30], Carrera et al. analyzed the static behavior of a beam with an airfoil-like section under a bending load by using TE elements. They pointed out that the use of higher-order theories improves the flexibility feature of the finite element model and the accuracy of the displacement, stress and strain distributions over the cross section. Beam formulation was employed to analyze the static behavior of thin-walled structures, bridge-like cross sections [31], and, furthermore, to present buckling and static analyses of laminated composite beams [32,33]. With regard to the TE model, it was found that the number of terms that have to be retained for each of the considered beam theories is closely related to the problem addressed. A comprehensive discussion of this issue is proposed by Carrera and Petrolo in Ref. [34]. Dynamic analyses have also been treated in many works. For instance, in Refs. [35–37] the dynamic characteristics of different beam sections and wing model were presented. Moreover, free vibration investigations have been carried out on hollow cylindrical reinforced structures [38], laminated composite [39], and functionally graded beams [40]. In literature, there are many other papers that report the features of CUF, but for a thorough and clear description it is recommended to refer to Ref. [41].

This paper is aimed at extending the CUF to the dynamic of rotors. The equations of motion are written in the rotating reference frame and they are solved by using FEM. The displacement fields within the refined finite elements are obtained by adopting Taylor's polynomials. In order to assess the new formulation, several linear analyses are carried out and the related results are compared with the solutions presented in the literature.

2 The Equations of Motion

When a structure is rotating, inertial forces and moments are observed. In this study, a beam that is free to rotate about its axis with a constant spin speed Ω is considered. Figure 1 shows the reference frame, which is rotating with the rotor and the cross section of the beam. The absolute velocity of the point P is the sum of the relative velocity and the transfer velocity.

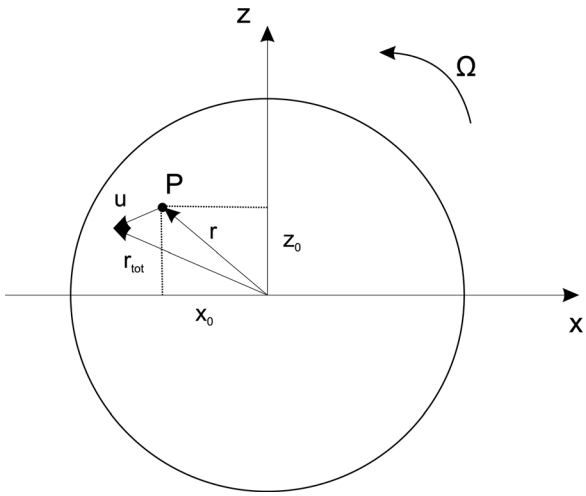

Fig. 1 Sketch of the rotating reference frame

$$\boldsymbol{v}_{\text{abs}} = \boldsymbol{v}_{\text{rel}} + \boldsymbol{v}_{tr} = \dot{\boldsymbol{u}} + \Omega \times \boldsymbol{r}_{\text{tot}} \tag{1}$$

$$\boldsymbol{\Omega} = \begin{bmatrix} 0 & 0 & \Omega \\ 0 & 0 & 0 \\ -\Omega & 0 & 0 \end{bmatrix}$$

where $\boldsymbol{u} = \{u_x \;\; u_y \;\; u_z\}^T$ is the displacement vector and $\boldsymbol{r}_{\text{tot}} = \boldsymbol{r} + \boldsymbol{u}$ is the distance of P from the neutral axis. The kinetic energy of the whole structure can be written as the following expression:

$$T = \frac{1}{2}\int_V \rho(\dot{\boldsymbol{u}}^T\dot{\boldsymbol{u}} + 2\boldsymbol{u}^T\boldsymbol{\Omega}^T\dot{\boldsymbol{u}} + \boldsymbol{u}^T\boldsymbol{\Omega}^T\boldsymbol{\Omega}\boldsymbol{u} + 2\dot{\boldsymbol{u}}^T\boldsymbol{\Omega}\boldsymbol{r} + 2\boldsymbol{u}^T\boldsymbol{\Omega}^T\boldsymbol{\Omega}\boldsymbol{r} + \boldsymbol{r}^T\boldsymbol{\Omega}^T\boldsymbol{\Omega}\boldsymbol{r})dV \tag{2}$$

Furthermore, the potential energy of the structure is

$$U = \frac{1}{2}\int_V (\boldsymbol{u}^T\boldsymbol{D}^T\boldsymbol{C}\boldsymbol{D}\boldsymbol{u})dV \tag{3}$$

where $\boldsymbol{D}$ is the matrix of linear differential operators and $\boldsymbol{C}$ is the matrix of material coefficients.

In order to obtain the motion equations, Hamilton's principle is used. In the usual form it states

$$\delta\int_{t_0}^{t_1}(T-U)dt = 0 \tag{4}$$

where δ is the virtual variation of the functional. Note that this expression leads to the well-known Euler–Lagrange equation

$$\int_{t_0}^{t_1}\left(\left(\frac{\partial(T-U)}{\partial\boldsymbol{u}} - \frac{d}{dt}\frac{\partial(T-U)}{\partial\dot{\boldsymbol{u}}}\right)\delta\boldsymbol{u}\right)dt = 0$$

Substituting Eqs. (2)–(3) into Eq. (4) and collecting the terms, we obtain the following equation:

$$\int_{t_0}^{t_1}\left(\int_V(\delta\boldsymbol{u}^T\rho\ddot{\boldsymbol{u}})dV + \int_V(\delta\boldsymbol{u}^T 2\rho\boldsymbol{\Omega}\dot{\boldsymbol{u}})dV + \int_V \delta\boldsymbol{u}^T(\boldsymbol{D}^T\boldsymbol{C}\boldsymbol{D} - \rho\boldsymbol{\Omega}^T\boldsymbol{\Omega})\boldsymbol{u}dV - \int_V(\delta\boldsymbol{u}^T\rho\boldsymbol{\Omega}^T\boldsymbol{\Omega}\boldsymbol{r})dV\right)dt = 0 \tag{5}$$

The above principle is satisfied in every time interval and for all possible perturbations if the equations of motion (Eq. (6)) are fulfilled.

$$\int_V \rho\ddot{\boldsymbol{u}} + 2\rho\boldsymbol{\Omega}\dot{\boldsymbol{u}} + (\boldsymbol{D}^T\boldsymbol{C}\boldsymbol{D} - \rho\boldsymbol{\Omega}^T\boldsymbol{\Omega})\boldsymbol{u}dV = \int_V \rho\boldsymbol{\Omega}^T\boldsymbol{\Omega}\boldsymbol{r}\,dV \tag{6}$$

3 The Unified Formulation

The CUF states that the displacement field, $\boldsymbol{u}(x,y,z,t)$, is an expansion of generic functions, $F_\tau(x,z)$ for the vector displacement, $\boldsymbol{u}_\tau(y)$

$$\boldsymbol{u}(x,y,z,t) = F_\tau(x,z)\boldsymbol{u}_\tau(y,t) \quad \tau = 1,2,\ldots,T \tag{7}$$

where T is the number of terms of the expansion and, in according to the generalized Einstein's notation, τ indicates summation. In this work, Eq. (7) consists of Taylor's polynomials that are functions of the coordinates of the cross section. For example, the second-order displacement field is

$$\begin{aligned} u_x &= u_{x_1} + xu_{x_2} + zu_{x_3} + x^2u_{x_4} + xzu_{x_5} + z^2u_{x_6} \\ u_y &= u_{y_1} + xu_{y_2} + zu_{y_3} + x^2u_{y_4} + xzu_{y_5} + z^2u_{y_6} \\ u_z &= u_{z_1} + xu_{z_2} + zu_{z_3} + x^2u_{z_4} + xzu_{z_5} + z^2u_{z_6} \end{aligned} \tag{8}$$

while the third-order displacement field becomes

$$\begin{aligned} u_x &= u_{x_1} + xu_{x_2} + zu_{x_3} + x^2u_{x_4} + xzu_{x_5} + z^2u_{x_6} + x^3u_{x_7} \\ &\quad + x^2zu_{x_8} + xz^2u_{x_9} + z^3u_{x_{10}} \\ u_y &= u_{y_1} + xu_{y_2} + zu_{y_3} + x^2u_{y_4} + xzu_{y_5} + z^2u_{y_6} + x^3u_{y_7} \\ &\quad + x^2zu_{y_8} + xz^2u_{y_9} + z^3u_{y_{10}} \\ u_z &= u_{z_1} + xu_{z_2} + zu_{z_3} + x^2u_{z_4} + xzu_{z_5} + z^2u_{z_6} + x^3u_{z_7} \\ &\quad + x^2zu_{z_8} + xz^2u_{z_9} + z^3u_{z_{10}} \end{aligned} \tag{9}$$

A remarkable feature is that classical beam theories are obtainable as particular cases of Taylor expansions. It should be noted that classical theories require reduced material stiffness coefficients to contrast Poisson's locking. Unless otherwise specified, for classical and first-order models, Poisson's locking is corrected according to Carrera and Giunta [41]. The stresses and the strains are grouped as it follows:

$$\begin{aligned} \boldsymbol{\epsilon}_p &= \{\varepsilon_{zz} \quad \varepsilon_{xx} \quad \varepsilon_{xz}\}^T \quad \boldsymbol{\sigma}_p = \{\sigma_{zz} \quad \sigma_{xx} \quad \sigma_{xz}\}^T \\ \boldsymbol{\epsilon}_n &= \{\varepsilon_{zy} \quad \varepsilon_{xy} \quad \varepsilon_{yy}\}^T \quad \boldsymbol{\sigma}_n = \{\sigma_{zy} \quad \sigma_{xy} \quad \sigma_{yy}\}^T \end{aligned} \tag{10}$$

The subscript "p" stands for terms lying on the cross section, while "n" stands for terms lying on the other planes, which are orthogonal to the cross section. The strain displacement relations and the Hooke's law are, respectively

$$\begin{aligned} \boldsymbol{\epsilon}_p &= \boldsymbol{D_p}\boldsymbol{u} \\ \boldsymbol{\epsilon}_n &= (\boldsymbol{D_{ny}} + \boldsymbol{D_{np}})\boldsymbol{u} \end{aligned} \tag{11}$$

$$\begin{aligned} \boldsymbol{\sigma}_p &= \boldsymbol{C}_{pp}\boldsymbol{\epsilon}_p + \boldsymbol{C}_{pn}\boldsymbol{\epsilon}_n \\ \boldsymbol{\sigma}_n &= \boldsymbol{C}_{np}\boldsymbol{\epsilon}_p + \boldsymbol{C}_{nn}\boldsymbol{\epsilon}_n \end{aligned} \tag{12}$$

For the sake of brevity, the explicit forms of the coefficients of the matrices $\boldsymbol{C}$ are not reported here, but they can be found in Tsai [42] or Reddy [43].

If a classical finite element technique is adopted with the purpose of easily dealing with arbitrary shaped cross sections, the generalized displacement vector becomes

$$\mathbf{u}_\tau(y,t) = N_i(y)\mathbf{q}_{\tau i}(t) \tag{13}$$

where $N_i(y)$ are the shape functions and $\mathbf{q}_{\tau i}(t)$ is the nodal displacement vector

$$\mathbf{q}_{\tau i}(t) = \left\{q_{u_{x_{\tau i}}} \quad q_{u_{y_{\tau i}}} \quad q_{u_{z_{\tau i}}}\right\}^T \tag{14}$$

4 Equations of Rotor Dynamics in CUF Form

The assumptions made in the above section allow us to rewrite the Eq. (5) by introducing the Eqs. (7), (11), (12), and (13)

$$\begin{aligned} \int_{t_0}^{t_1} &\left(\delta\boldsymbol{q}_{\tau i}^T\boldsymbol{M}^{ij\tau s}\ddot{\boldsymbol{q}}_{sj} + \delta\boldsymbol{q}_{\tau i}^T\boldsymbol{G}^{ij\tau s}\dot{\boldsymbol{q}}_{sj}\right. \\ &\left. + \delta\boldsymbol{q}_{\tau i}^T\left(\boldsymbol{K}^{ij\tau s} - \boldsymbol{K}_{\boldsymbol{\Omega}}^{ij\tau s}\right)\boldsymbol{q}_{sj} + \delta\boldsymbol{q}_{\tau i}^T\boldsymbol{F}_{\boldsymbol{\Omega}}^{i\tau}\boldsymbol{r}\right)dt = 0 \end{aligned} \tag{15}$$

The matrices are written in form of the fundamental nuclei and their explicit forms are

$$\begin{aligned} \boldsymbol{M}^{ij\tau s} &= I_l^{ij} \lhd (F_\tau\rho\boldsymbol{I}F_s) \rhd \\ \boldsymbol{G}^{ij\tau s} &= I_l^{ij} \lhd (F_\tau\rho\boldsymbol{I}F_s) \rhd 2\boldsymbol{\Omega} \\ \boldsymbol{K}_{\boldsymbol{\Omega}}^{ij\tau s} &= I_l^{ij} \lhd (F_\tau\rho\boldsymbol{I}F_s) \rhd \boldsymbol{\Omega}^T\boldsymbol{\Omega} \\ \boldsymbol{K}^{ij\tau s} &= I_l^{ij} \lhd \boldsymbol{D}_{np}^T(F_\tau\boldsymbol{I})\left[\boldsymbol{C}_{np}\boldsymbol{D}_p(F_s\boldsymbol{I}) + \boldsymbol{C}_{nn}\boldsymbol{D}_{np}(F_s\boldsymbol{I})\right] \\ &\quad + \boldsymbol{D}_p^T(F_\tau\boldsymbol{I})\left[\boldsymbol{C}_{pp}\boldsymbol{D}_p(F_s\boldsymbol{I}) + \boldsymbol{C}_{pn}\boldsymbol{D}_{np}(F_s\boldsymbol{I})\right] \rhd \\ &\quad + I_l^{ij,y} \lhd \left[\boldsymbol{D}_{np}^T(F_\tau\boldsymbol{I}) + \boldsymbol{D}_p^T(F_\tau\boldsymbol{I})\boldsymbol{C}_{pn}\right]F_s \rhd + \boldsymbol{I}_{Ay} \\ &\quad + I_l^{i,yj}\boldsymbol{I}_{Ay}^T \lhd F_\tau\left[\boldsymbol{C}_{np}\boldsymbol{D}_p(F_s\boldsymbol{I}) + \boldsymbol{C}_{nn}\boldsymbol{D}_{np}(F_s\boldsymbol{I})\right] \rhd \\ &\quad + I_l^{i,yj,y}\boldsymbol{I}_{Ay}^T\boldsymbol{I}_{Ay} \lhd F_\tau\boldsymbol{C}_{nn}F_s \rhd \\ \boldsymbol{F}_{\boldsymbol{\Omega}}^{i\tau} &= I_l^i \lhd F_\tau\rho\boldsymbol{r} \rhd \boldsymbol{\Omega}^T\boldsymbol{\Omega} \end{aligned} \tag{16}$$

where

$$\boldsymbol{I}_{Ay} = \begin{bmatrix} 0 & 0 & 1 \\ 1 & 0 & 0 \\ 0 & 1 & 0 \end{bmatrix} \quad \lhd \ldots \rhd = \int_A \ldots\, dA \tag{17}$$

$$\left(I_l^i, I_l^{ij}, I_l^{ij,y}, I_l^{i,yj}, I_l^{i,yj,y}\right) = \int_l (N_i, N_iN_j, N_iN_{j,y}, N_{i,y}N_j, N_{i,y}N_{j,y})dy \tag{18}$$

In addition to the mass matrix $\boldsymbol{M}^{ij\tau s}$ and the stiffness matrix $\boldsymbol{K}^{ij\tau s}$, the expression of the kinetic energy introduces other three terms

- the coriolis matrix $\boldsymbol{G}^{ij\tau s}$
- the spin softening matrix $\boldsymbol{K}_{\boldsymbol{\Omega}}^{ij\tau s}$
- the load vector $\boldsymbol{F}_{\boldsymbol{\Omega}}^{i\tau}$

To obtain the natural frequencies and the normal modes of the rotor, we have to solve the homogeneous equations

$$\boldsymbol{M}\ddot{\boldsymbol{q}} + \boldsymbol{G}_\Omega\dot{\boldsymbol{q}} + (\boldsymbol{K} - \boldsymbol{K}_\Omega)\boldsymbol{q} = 0 \tag{19}$$

It must be highlighted that the softening contribution appears in the Eq. (19) since, in this paper, the reference frame adopted is rotating with the structure.

Now, it is possible to assume a periodic function as solution

$$\boldsymbol{q} = \boldsymbol{q}e^{i\omega t} \tag{20}$$

Substituting Eq. (20) and its derivative in Eq. (19), it becomes

$$\boldsymbol{q}e^{i\omega t}\left[(\boldsymbol{K} - \boldsymbol{K}_\Omega) + (\boldsymbol{G}_\Omega)i\omega - (\boldsymbol{M})\omega^2\right] = 0 \tag{21}$$

The Eq. (21) represents a quadratic eigenvalues problem (QEP) where the imaginary values ω are related to the natural frequencies and to the damping of the rotor system. A possible solution

can be made by transforming the QEP of a generic order R (where R is the number of degrees of freedom, DOF) in a classical 'linear' eigenvalues problem of order $2 \times R$.

$$\begin{cases} \boldsymbol{M}\ddot{\boldsymbol{q}} + \boldsymbol{G}_{\Omega}\dot{\boldsymbol{q}} + (\boldsymbol{K} - \boldsymbol{K}_{\Omega})\boldsymbol{q} = 0 \\ -\dot{\boldsymbol{q}} + \dot{\boldsymbol{q}} = 0 \end{cases} \tag{22}$$

now, by introducing

$$\boldsymbol{a} = \begin{Bmatrix} \boldsymbol{q} \\ \dot{\boldsymbol{q}} \end{Bmatrix} \quad \dot{\boldsymbol{a}} = \begin{Bmatrix} \dot{\boldsymbol{q}} \\ \ddot{\boldsymbol{q}} \end{Bmatrix} \tag{23}$$

the equations of motion assume the following form:

$$\boldsymbol{R}\dot{\boldsymbol{a}} + \boldsymbol{T}\boldsymbol{a} = 0 \tag{24}$$

Now, by substituting Eq. (20) in Eq. (24) we obtain

$$\frac{\boldsymbol{R}}{\boldsymbol{T}} - \frac{1}{i\omega}\boldsymbol{I} = 0 \tag{25}$$

where

$$\boldsymbol{T}^{-1}\boldsymbol{R} = \begin{bmatrix} (\boldsymbol{K} - \boldsymbol{K}_{\Omega})^{-1}\boldsymbol{G}_{\Omega} & (\boldsymbol{K} - \boldsymbol{K}_{\Omega})^{-1}\boldsymbol{M} \\ -\boldsymbol{I} & \boldsymbol{0} \end{bmatrix} \tag{26}$$

The problem in Eq. (25) is in the classical form and it can be solved with the standard eigensolvers.

5 Numerical Results

In order to assess the theory of the previous sections, several illustrative examples are presented. The boundary conditions and the ratio between the cross section dimensions are assumed to be a problem's parameter. If not otherwise declared, ten finite elements are used for the discretization along the y-axis. With the purpose of enabling a general application of results, they are presented in nondimensional form by adopting the following nondimensional natural frequency and spinning speed parameters:

$$\omega^* = \frac{\omega}{\omega_0}, \quad \Omega^* = \frac{\Omega}{\omega_0}, \quad \omega_0 = \sqrt{\frac{\sqrt{EJ_{xx}EJ_{yy}}}{\rho AL^4}}$$

where J_{xx}, J_{zz} are the moments of inertia in the two principal planes, E is the Young's modulus, A the area of the cross section, and L the length of the beam. In the first example, the dynamic behavior of a beam with $J_{xx} = J_{zz}$ which is subjected to different boundaries conditions is investigated. Equation (27) has been exploited for comparison purposes and the relative results are reported in graphical form in Fig. 2.

$$\omega_{\text{ref}} = \lambda^2 \sqrt{\frac{EI}{\rho AL^4}} \mp \Omega \tag{27}$$

where λ is a coefficient depending on the boundary conditions.

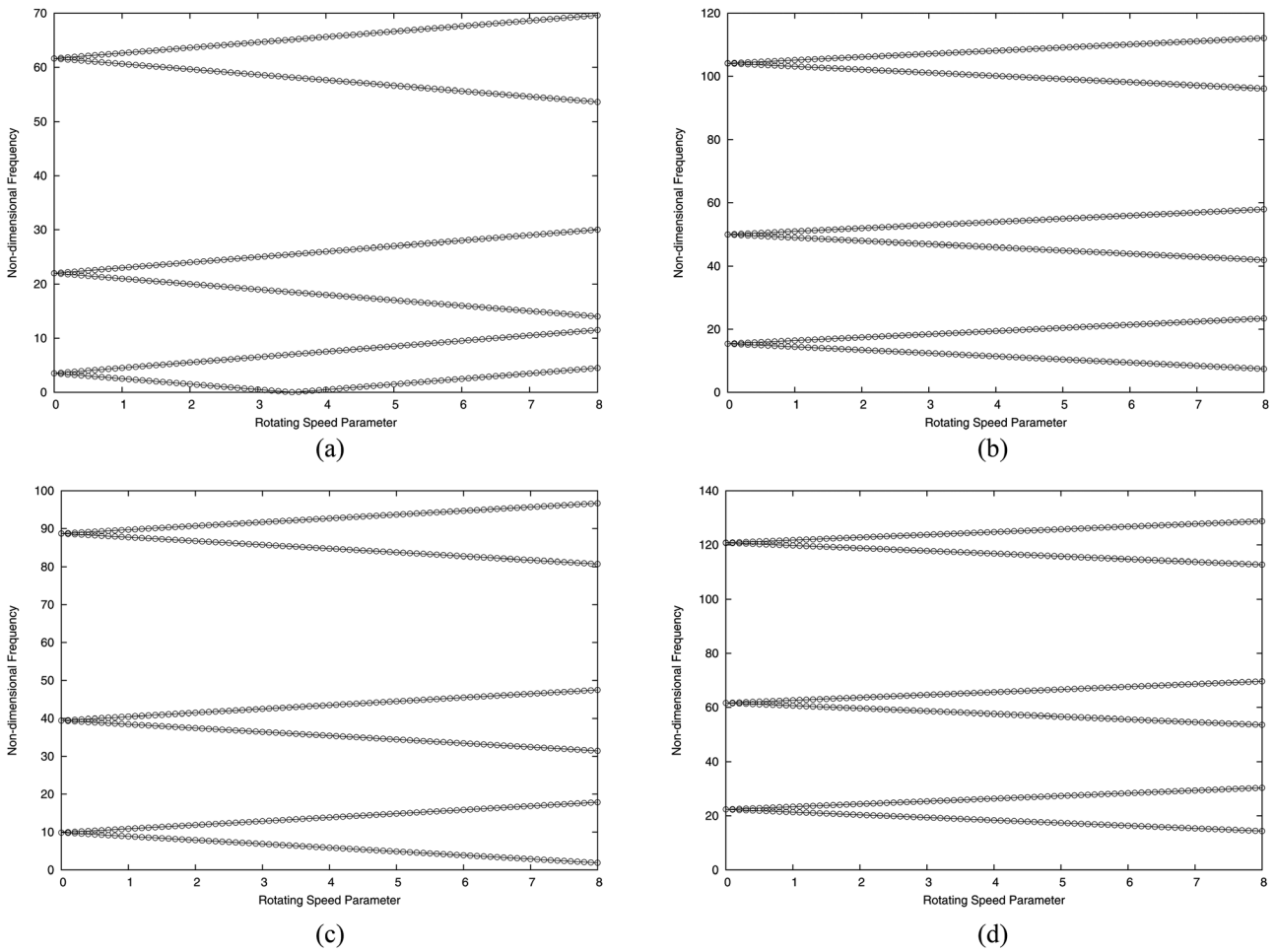

Fig. 2 The variation of nondimensional natural frequencies with spinning speed parameter for a beam (J_{xx}, J_{zz}) subjected to several boundary conditions ('lines': Eq. (27); '⊙': CUF). (*a*) Clamped-free, (*b*) clamped-supported, (*c*) supported-supported, (*d*) clamped-clamped.

Table 1 Frequency ratios of a cantilever spinning beam with $J_{xx} = J_{zz}$

Ω^*	Theory	ω_1^*	ω_2^*	ω_3^*	ω_4^*	ω_5^*	ω_6^*
0	[3]	3.516	3.516	22.034	22.034	61.697	61.967
	Present	3.510	3.510	21.992	21.992	61.551	61.551
2	[3]	1.516	5.516	20.034	24.034	59.697	63.697
	Present	1.510	5.510	19.995	23.992	59.559	63.552
3.51	[3]	0	7.016	18.534	25.534	58.197	65.197
	Present	0	7.020	18.486	25.500	58.052	65.059
4	[3]	—	7.516	18.034	26.034	57.697	65.697
	Present		7.509	17.996	25.990	57.563	65.548

As can be seen, the results derived by the unified formulation match those of the analytical solutions for every type of boundary condition. Since the effects of shear deformation and rotatory inertia are considered to be small for this type of rotor, the study was conducted using the Euler–Bernoulli theory. In Table 1, some values of nondimensional natural frequency at different spinning speed parameters are compared with those obtained by Banerjee and Su in Ref. [3] for the cantilever beam. It should be noted that the frequencies are very close to those of the reference and especially the value of the critical speed at which the beam becomes unstable. In the same work, Banerjee and Su [3] presented the results related to beams with rectangular cross sections. Figure 3 shows how the first two flexural natural frequencies are affected by the ratio between the main cross section dimensions, b/h, when the rotating speed is changing. The reference solutions are obtained by Eq. (28), in which $\tilde{\omega}_x$ and $\tilde{\omega}_z$ are the natural frequencies at standstill.

$$\omega_{x,z} = \sqrt{\frac{1}{2}\left\{ -(\tilde{\omega}_x^2 + \tilde{\omega}_z^2 + 2\Omega^2) \pm \sqrt{(\tilde{\omega}_x^2 - \tilde{\omega}_z^2)^2 + 8\Omega^2(\tilde{\omega}_x^2 + \tilde{\omega}_z^2)} \right\}} \tag{28}$$

As can be seen, the behaviors of the frequencies in the two principal planes are very different. In fact, the first decreases until it becomes zero, whereas the second continues to increase. It is important to note that, for these values of *aspect − ratio*, the flexural normal modes in the two planes are alternated. On the contrary, when the width becomes much smaller than the height, the relationship for the frequency ratios undergoes an observable change. For instance, if $b = 0.1\,\mathrm{h}$, the first two mode frequency ratios in the x direction are smaller than the first one in the z direction. This difference is shown in Fig. 4, where the first seven frequency ratios are presented. For the last case, in Table 2, the results obtained with CUF are compared with the numerical values of frequency ratios presented in Ref. [3]. As said before, the effects of shear deformation can be disregarded when the shaft is very thin, but if this approximation is no longer valid, other structural models are needed. In the following test case, a moderate thick cylindrical beam simply supported is analyzed. The length and the radius are assumed to be equal to 10 m and 0.25 m, respectively. The material has the Young's modulus equal to 210 GPa whereas the Poisson coefficient and the density are 0.3 and 7800 kg/m^3. The results in Table 3 are compared with those provided by Curti et al. [7], who proposed an analytical procedure based on DSM by including the effects of the shear deformation of the shaft. The results agree with the reference solutions and it must be highlighted that the effect of the shear deformation plays an important role for moderate thick structures and refined theories are able to detect this phenomena.

Although in this paper the centrifugal stiffening term is not considered, a rotating thin disk fixed on a flexible shaft clamped at each extremity was studied with the purpose to evaluate the capabilities of the higher order 1D finite elements. The centrifugal stiffening contribution becomes very important when a deformable body is rotating but, in this case, the aim is to compare the advanced one-dimensional elements with the classical beam model. The length and the radius of the shaft are assumed to be $L_s = 0.40$ m and $R_s = 0.01$ m whereas those of the disk are $L_d = 0.005$ m and $R_d = 0.15$ m. The material is considered isotropic with the Young modulus, E, equal to 207 GPa and the density, ρ, 7860 kg/m^3. The structure is shown in Fig. 5. In Table 4, the frequencies related to the first ten normal modes at standstill computed by adopting the solid finite elements (HEX8) are compared with those calculated with the higher order theories. The second and third modes are two global bending modes of the

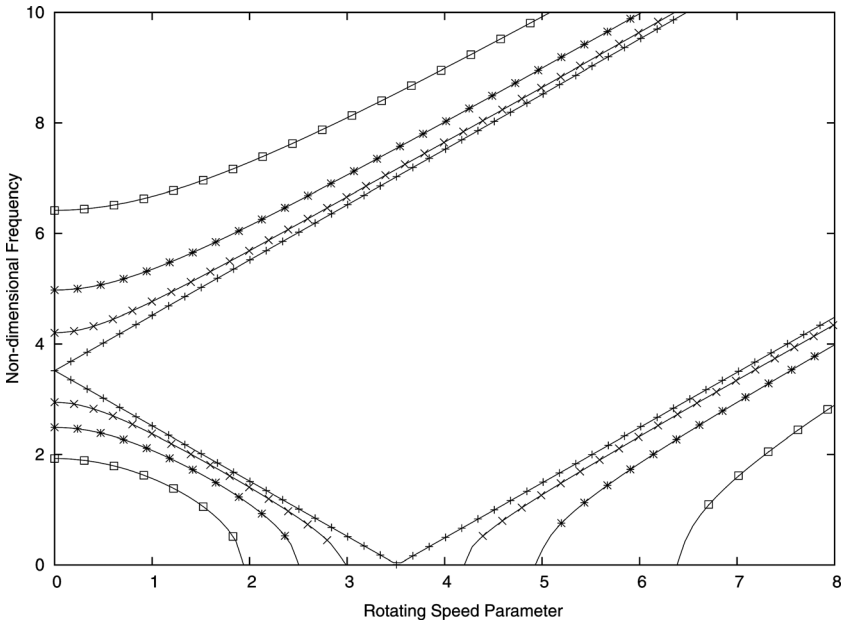

Fig. 3 The first two frequency ratios w_1^* and w_2^* as functions of the spinning speed ratio for various values of aspect − ratio ('−': Eq. (28); '+': $b/h = 1$; '×': $b/h = 0.7$; '*': $b/h = 0.5$; '□': $b/h = 0.3$)

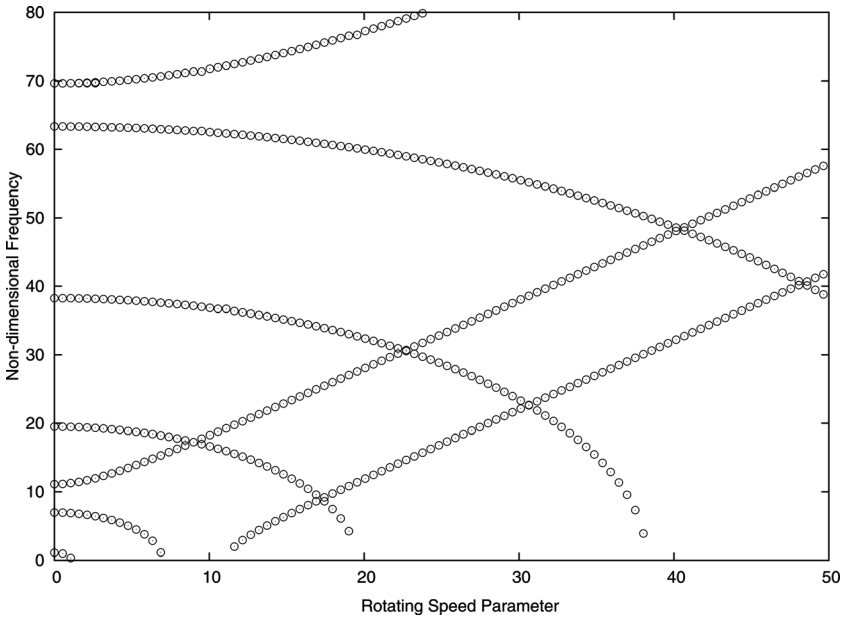

Fig. 4 The first seven frequency ratios w_1^*–w_7^* as functions of the spinning speed ratio for aspect-ratio equal to 0.1

Table 2 Frequency ratios of a cantilever spinning beam with rectangular cross section ($b = 0.1\,h$)

Ω*	Theory	ω_1^*	ω_2^*	ω_3^*	ω_4^*
0	[3]	1.1119	6.9680	11.119	19.511
	Present	1.1114	6.9658	11.119	19.508
1.11	[3]	0	6.8623	11.307	19.473
	Present	0	6.8732	11.284	19.475
2	[3]	0	6.6637	11.632	19.404
	Present	0	6.6611	11.633	19.401
4	[3]	—	5.6679	12.900	19.080
	Present	—	5.6638	12.901	19.077
6	[3]	—	3.4910	14.536	18.530
	Present	—	3.4818	14.538	18.526
7.1	[3]	—	0	15.526	18.118
	Present	—	0	15.524	18.116
8	[3]	—	—	16.3367	17.7348
	Present	—	—	16.3399	17.7310

Table 3 Forward critical speeds predicted by CUF for the test case of a simply supported shaft

Mode number	[7]	EBBM	FSDT	$N = 1$
1	63.869	63.699	63.550	63.550
2	253.769	255.001	252.449	252.373
3	564.741	573.379	564.299	564.180
4	989.050	1019.405	988.400	992.300
5	1516.866	1599.400	1519.259	1519.000

Note: EBBM stands for Euler–Bernoulli beam model. FSDT stands for first-order shear deformation theory.

structure and even the Euler–Bernoulli beam model (EBBM) and the first-order shear deformation theory (FSDT) are able to detect this behavior, but the relative error on the computation of these two frequencies is about of 50%. However, it must be noted that although the higher order models are used, this error is the highest (25% with TE7). When the components of the displacement field are enriched, the flexibility of the disk is enhanced and the modal

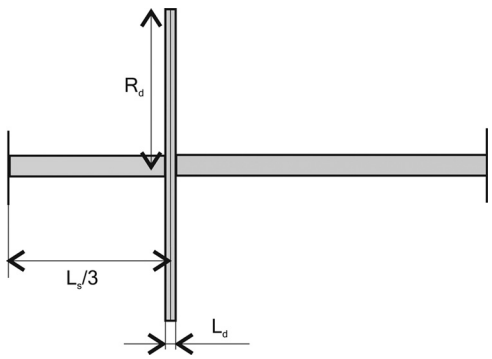

Fig. 5 The rotating structure

shapes 2 and 3 involve both flexural and shell-like deformations. In order to achieve better results, the displacement theory should be further improved by increasing the number of terms of the Taylor-like expansion. On the other hand, the error related to the fifth and sixth normal modes increases about up to 60%. These two modes of deformation are affected by the flexibility of the disk and the error decreases below to the 20% only with the fifth-order theory. Furthermore, if a sixth-order theory is adopted, the values of the frequencies related to the shell-like modes of the disk are close to the reference solutions and the relative errors are below 10%. In light of these results, it is clear that classical beam models are not suitable for analyzing the dynamic behavior of flexible rotors. Figure 6 shows the Campbell's diagrams obtained with several 1D theories. It is clear that if the order of the polynomials increases, new modal shapes are detected and it is possible show how their related frequencies change with the spinning speed. Furthermore, in these graphs, it is possible to distinguish some interesting points, whose values of frequency and rotation speed are listed in Table 5. The points "A" and "B" are two critical values of Ω. It must be highlighted that with both the EBBM and the FSDT, only the speed indicated with "B" is detected. Moreover by adopting several structural models, its value does not change (about 678 rad/s) despite the fact that the related frequency at standstill markedly decreases with the increasing of the approximation order. On the contrary, the first critical speed ("A")

Table 4 Natural frequencies of the structure of Fig. 5

Theory	1_T	$2_B - 3_B$	4_S	$5_B - 6_B$	$7_S - 8_S$	$9_S - 10_S$
Solid	677.45	881.34	1384.18	1527.63	1893.24	4439.32
EBBM	—	1313.12^{48}	—	2500.83^{63}	—	—
FSDT	—	1304.32^{48}	—	2456.53^{60}	—	—
$N = 1$	678.52^{0}	1304.32^{48}	—	2456.53^{60}	—	—
2	678.52^{0}	1315.19^{49}	1954.32^{41}	2486.13^{62}	2119.88^{11}	—
3	678.45^{0}	1288.42^{46}	1949.42^{41}	2175.05^{42}	2112.46^{11}	4945.43^{11}
4	678.45^{0}	1287.86^{46}	1533.59^{11}	2171.40^{42}	1994.47^{5}	4934.37^{10}
5	678.26^{0}	1202.35^{36}	1532.72^{11}	1794.35^{17}	1993.46^{5}	4355.88^{2}
6	678.26^{0}	1200.90^{36}	1487.41^{7}	1791.08^{17}	1993.27^{5}	4351.48^{3}
7	677.95^{0}	1108.10^{25}	1487.29^{7}	1660.70^{9}	1992.33^{5}	4309.51^{3}

Note: The subscripts A, B, S stand for axial, bending, and shell-like mode; the superscript is the relative error (%).

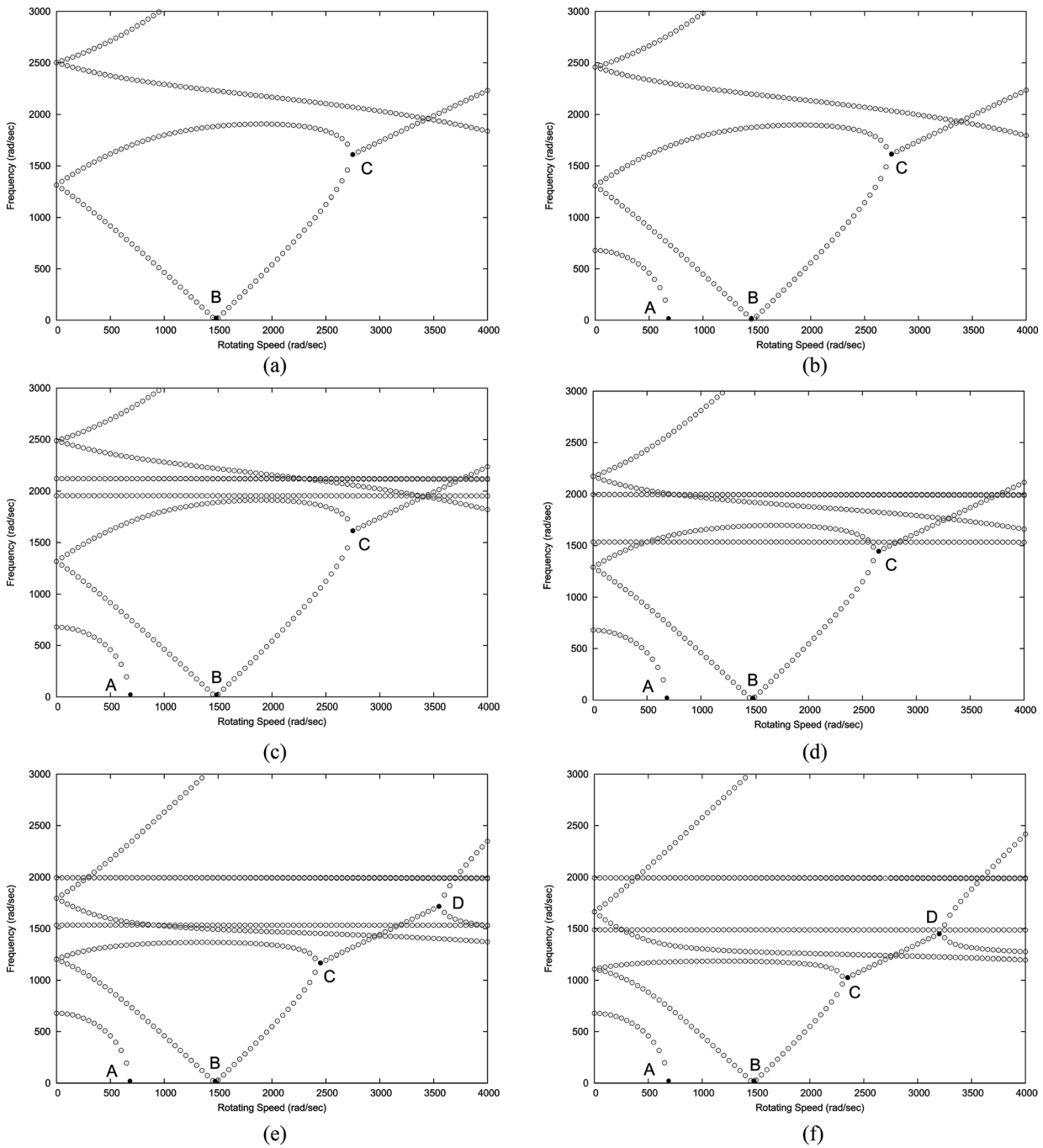

Fig. 6 The variation of natural frequencies with the spinning speed for the structure of Fig. 5. (*a*) EBBM, (*b*) TE1, (*c*) TE2, (*d*) TE4, (*e*) TE5, and (*f*) TE7.

Table 5 Frequencies (rad/s) and rotational speed (rad/s) related to the points of the graph 7

		EBBM	$N=1$	$N=2$	$N=4$	$N=5$	$N=7$
A	ω	—	0.0	0.0	0.0	0.0	0.0
	Ω	—	678	678	678	678	678
B	ω	0.0	0.0	0.0	0.0	0.0	0.0
	Ω	1477	1476	1476	1476	1476	1476
C	ω	1610.5	1614.0	1614.1	1444.8	1168.7	1025.7
	Ω	2750	2750	2750	2650	2450	2350
D	ω	—	—	—	—	1716.3	1449.0
	Ω	—	—	—	—	3550	3200

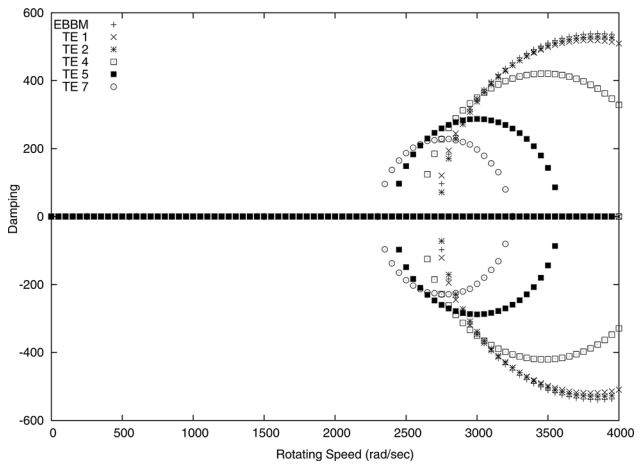

Fig. 7 The variation of damping with the spinning speed for the structure of Fig. 5

is individuated only with the higher-order theories but, also in this case, its value remains almost constant. As the Ω increases above the critical speeds, the modes of whirling are stable until the point "C." This point is the beginning of the self-excited range where the frequencies are complex conjugate. When the real part is negative, the rotor system is unstable and it is moving in an ellipse at the frequency ω. The self-excited range finishes at point "D." In the limits considered of speed, the aforementioned point appears only if the theory order is higher than 4, therefore, the instability region delimited by the rotating speeds of the points "C" and "D" is reduced. The self-excited range is easily individuated by observing the graph that reports the damping as a function of spin speed (Fig. 7). The two circular arches represent the real parts of the complex conjugates, which are solutions of the motion equations. In addition to the reduction of the instability range, the maximum values of damping are also lower with the increasing of the theory order. This behavior is only detected by the refined models. This aspect will be properly investigated in future works, in which the centrifugal stiffening will be included for studying correctly the deformable rotors.

6 Conclusion

In the present work, a CUF was developed and extended for studying the dynamic of rotors. By using the Hamilton's principle the equations of motion are derived and solved with the FEM. Many kinds of rotors were considered to assess the new theory and the related results were compared with those found in literature. Higher order elements were tested on a shaft with a disk with the purpose of highlighting the differences introduced by the refined displacement models. In the light of the results it is possible to make the following remarks:

- the use of finite elements based on the classical beam model leads to results that agree very well with reference solutions for all boundary conditions and cross sections considered;
- when the rotation speed is null, the refined models detect new modes of deformation and their relative frequencies with good accuracy;
- with the further introduction of the centrifugal stiffening contribution, the structural models proposed in this work appear able to describe the dynamics of the spinning structures with a high deformability.

Future work could be direct to analyze other aspects of rotating structures, among these the nonlinear geometrical effects due to large deformations of thin-walled shafts and disks appear of particular interest to the authors.

References

[1] Bauer, H. F., 1980, "Vibration of a Rotating Uniform Beam, Part 1: Orientation in the Axis of Rotation," J. Sound Vib., **72**, pp. 177–189.
[2] Chen, M. L., and Liao, Y. S., 1991, "Vibrations of Pretwisted Spinning Beams Under Axial Compressive Loads With Elastic Constraints," J. Sound Vib., **147**, pp. 497–513.
[3] Banerjee, J. R., and Su, H., 2004, "Development of a Dynamic Stiffness Matrix for Free Vibration Analysis of Spinning Beams," Comput. Struct., **82**, pp. 2189–2197.
[4] Zu, J. W. Z., and Han, R. P. S., 1992, "Natural Frequencies and Normal Modes of a Spinning Timoshenko Beam With General Boundary Conditions," ASME J. Appl. Mech., **59**, pp. 197–204.
[5] Choi, S.-T., Wu, J.-D., and Chou, Y.-T., 2000, "Dynamic Analysis of a Spinning Timoshenko Beam by the Differential Quadrature Method," AIAA J., **38**, pp. 851–856.
[6] Curti, G., Raffa, F. A., and Vatta, F., 1991, "The Dynamic Stiffness Matrix Method in the Analysis of Rotating Systems," Tribol. Trans., **34**, pp. 81–85.
[7] Curti, G., Raffa, F. A., and Vatta, F., 1992, "An Analytical Approach to the Dynamics of Rotating Shafts," Meccanica, **27**, pp. 285–292.
[8] Sheu, G. J., and Yang, S. M., 2005, "Dynamic Analysis of a Spinning Rayleigh Beam," Int. J. Mech. Sci., **47**, pp. 157–169.
[9] Sheu, H.-C., and Chen, L.-W., 2000, "A Lumped Mass Model for Parametric Instability Analysis of Cantiever Shaft-Disc System," J. Sound Vib., **234**, pp. 331–348.
[10] Singh, S. P., and Gupta, K., 1996, "Compostite Shaft Rotordynamic Analysis Using a Layerwise Theory," J. Sound Vib., **191**, pp. 739–756.
[11] Ramezani, S., and Ahmadian, M. T., 2009, "Free Vibration Analysis of Rotating Laminated Cylindrical Shells Under Different Boundary Conditions Using a Combination of the Layerwise Theory and Wave Propagation Approach," Trans. B: Mech. Eng., **16**(2), pp. 168–176.
[12] Banerjee, J. R., and Su, H., 2006, "Dynamic Stiffness Formulation and Free Vibration Analysis of a Spinning Composite Beam," Comput. Struct., **84**, pp. 1208–1214.
[13] Song, O., Librescu, L., and Jeong, N.-H., 2002, "Vibration and Stability Control of Composite Rotating Shaft Via Structural Tailoring and Piezoeletric Strain Actuation," J. Sound Vib., **257**, pp. 503–525.
[14] Librescu, L., Oh, S. Y., and Song, O., 2004, "Spinning Thin-Walled Beams Made of Functionally Graded Materials: Modeling, Vibration and Instability," Eur. J. Mech. A/Solids, **23**, pp. 499–515.
[15] Oh, S. Y., Librescu, L., and Song, O., 2005, "Vibration and Instability of Functionally Graded Circular Cylindrical Spinning Thin-Walled Beams," J. Sound Vib., **285**, pp. 1071–1091.
[16] Na, S., Yoon, H., and Librescu, L., 2006, "Effect of Taper Ratio on Vibration and Stability of a Composite Thin-Walled Spinning Shaft," Thin-Walled Struct., **44**, pp. 362–371.
[17] Genta, G., and Tonoli, A., 1996, "A Harmonic Finite Element for the Analysis of Flexural, Torsional and Axial Rotordynamics Behaviour of Discs," J. Sound Vib., **196**, pp. 19–43.
[18] Genta, G., Feng, C., and Tonoli, A., 2010, "Dynamics Behavior of Rotating Bladed Discs: A Finite Element Formulation for the Study of Second and Higher Order Harmonics," J. Sound Vib., **329**, pp. 5289–5306.
[19] Jang, G. H., and Lee, S. H., 2002, "Free Vibration Analysis of a Spinning Flexible Disk-Spindle System Supported by Ball Bearing and Flexible Shaft Using the Finite Element Method and Substructure Synthesis," J. Sound Vib., **251**, pp. 59–78.
[20] Guo, D., Zheng, Z., and Chu, F., 2002, "Vibration Analysis of Spinning Cylindrical Shells by Finite Element Method," Int. J. Solids Struct., **39**, pp. 725–739.
[21] Combescure, D., and Lazarus, A., 2008, "Refined Finite Element Modelling for the Vibration Analysis of Large Rotating Machines: Application to the Gas Turbine Modular Helium Reactor Power Conversion Unit," J. Sound Vib., **318**, pp. 1262–1280.
[22] Rao, J., 1985, *Rotor Dynamics*, Wiley Eastern, Delhi, India.
[23] Genta, G., 2005, *Dynamics of Rotating Systems*, Springer, New York.
[24] Carrera, E., 2002, "Theories and Finite Elements for Multilayered, Anisotropic, Composite Plates and Shells," Arch. Comput. Methods Eng., **9**(2), pp. 87–140.

[25] Carrera, E., 2003, "Theories and Finite Elements for Multilayered Plates and Shells: A Unified Compact Formulation With Numerical Assessment and Benchmarking," Arch. Comput. Methods Eng., **10**(3), pp. 216–296.
[26] Ballhause, D., D'Ottavio, M., Kröplin, B., and Carrera, E., 2004, "A Unified Formulation to Assess Multilayered Theories for Piezoelectric Plates," Comput. Struct., **83**, pp. 1217–1235.
[27] Carrera, E., 2004, "Assessment of Theories for Free Vibration Analysis of Homogeneous and Multilayered Plates," Shock Vib., **3–4**, pp. 261–270.
[28] Carrera, E., and Giunta, G., 2010, "Refined Beam Theories Based on a Unified Formulation," Int. J. Appl. Mech., **2**, pp. 117–143.
[29] Carrera, E., Petrolo, M., Wenzel, C., Giunta, G., and Belouettar, S., 2009, "Higher Order Beam Finite Elements With Only Displacement Degrees of Freedom," Proceedings of the XIX Conference of Italian Association of Applied and Theoretic Mechanics (AIMETA), Ancona, Italy, September 14–17, pp. 1–11.
[30] Carrera, E., Giunta, G., Nali, P., and Petrolo, M., 2010, "Refined Beam Elements With Arbitrary Cross-Section Geometries," Comput. Struct., **88**(5–6), pp. 283–293.
[31] Carrera, E., Petrolo, M., and Zappino, E., 2012, "Performance of CUF Approach to Analyze the Structural Behavior of Slender Bodies," J. Struct. Eng., **138**, pp. 285–298.
[32] Ibrahim, S. M., Carrera, E., Petrolo, M., and Zappino, E., 2012, "Buckling of Composite Thin Walled Beams by Refined Theory," Compos. Struct., **94**, pp. 563–570.
[33] Catapano, A., Giunta, G., Belouettar, S., and Carrera, E., 2011, "Static Analysis of Laminated Beams Via a Unified Formulation," Compos. Struct., **94**, pp. 75–83.
[34] Carrera, E., and Petrolo, M., 2011, "On the Effectiveness of Higher-Order Terms in Refined Beam Theories," ASME J. Appl. Mech., **78**(3), p. 021013.
[35] Carrera, E., Petrolo, M., and Nali, P., 2011, "Unified Formulation Applied to Free Vibrations Finite Element Analysis of Beams With Arbitrary Section," Shock Vib., **18**(3), pp. 485–502.
[36] Petrolo, M., Zappino, E., and Carrera, E., 2012, "Refined Free Vibration Analysis of One-Dimensional Structures With Compact and Bridge-Like Cross-Sections," Thin-Walled Struct., **56**, pp. 49–61.
[37] Carrera, E., Petrolo, M., and Varello, A., 2011, "Advanced Beam Formulations for Free Vibration Analysis of Conventional and Joined Wings," J. Aerosp. Eng., **25**(2), pp. 282–293.
[38] Carrera, E., Zappino, E., and Filippi, M., 2013, Free Vibration Analysis of Thin– Walled Cylinders Reinforced With Longitudinal and Transversal Stiffeners," ASME J. Vib. Acoust. **135**(1), p. 011019.
[39] Giunta, G., Biscani, F., Belouettar, S., Ferreira, A. J. M., and Carrera, E., 2013, "Free Vibration Analysis of Composite Beams Via Refined Theories," Composites, Part B, **44**, pp. 540–552.
[40] Giunta, G., Crisafulli, D., Belouettar, S., and Carrera, E., 2011, "Hierarchical Theories for the Free Vibration Analysis of Functionally Graded Beams," Compos. Struct., **94**, pp. 68–74.
[41] Carrera, E., Giunta, G., and Petrolo, M., 2011, *Beam Structures. Classical and Advanced Theories*, Wiley, New York.
[42] Tsai, S. W., 1988, *Composites Design*, 4th ed., Think Composites, Dayton, OH.
[43] Reddy, J. N., 2004, *Mechanics of Laminated Composite Plates and Shells. Theory and Analysis*, 2nd ed., CRC Press, Boca Raton, FL.